HHS Public Access

Author manuscript

Mol Cancer Ther. Author manuscript; available in PMC 2020 January 01.

Published in final edited form as:

Mol Cancer Ther. 2019 January ; 18(1): 51–61. doi:10.1158/1535-7163.MCT-18-0104.

A Unique Non-Saccharide Mimetic of Heparin Hexasaccharide Inhibits Colon Cancer Stem Cells via p38 MAP Kinase Activation.

Rio S. Boothello[1,2], **Nirmita J. Patel**[2,3,4], **Chetna Sharon**[2], **Elsamani I. Abdelfadiel**[3], **Shravan Morla**[3,4], **Donald F. Brophy**[5], **H Robert Lippman**[2], **Umesh R. Desai**[3,4], and **Bhaumik B. Patel**[*,1,2]

[1]Division of Hematology and Oncology, Department of Internal Medicine, Massey Cancer Center, Virginia Commonwealth University, Richmond, VA 23298

[2]McGuire VA Medical Center, Richmond, VA 23249

[3]Institute for Structural Biology, Drug Discovery and Development, Virginia Commonwealth University, Richmond, VA 23298

[4]Department of Medicinal Chemistry, Virginia Commonwealth University, Richmond, VA 23298

[5]Department of Pharmacotherapy and Outcomes Sciences, Virginia Commonwealth University, Richmond, VA 23298

Abstract

Targeting of cancer stem cells (CSCs) is expected to be a paradigm-shifting approach for the treatment of cancers. Cell surface proteoglycans bearing sulfated glycosaminoglycan (GAG) chains are known to play a critical role in the regulation of stem cell fate. Here, we show for the first time that G2.2, a sulfated non-saccharide GAG mimetic (NSGM) of heparin hexasaccharide, selectively inhibits colonic CSCs in vivo. G2.2 reduced CSCs (CD133+/CXCR4+, Dual hi) induced HT-29 and HCT 116 colon xenografts' growth in a dose-dependent fashion. G2.2 also significantly delayed the growth of colon xenograft further enriched in CSCs following oxaliplatin and 5-fluorouracil treatment compared to vehicle-treated xenograft controls. In fact, G2.2 robustly inhibited CSCs abundance (measured by levels of CSC markers, e.g., CD133, DCMLK1, LGR5, LRIG1) and self-renewal (quaternary spheroids) in colon cancer xenografts. Intriguingly, G2.2 selectively induced apoptosis in the Dual hi CSCs in vivo eluding to its CSC targeting effects. More importantly, G2.2 displayed none to minimal toxicity as observed through morphologic and biochemical studies of vital organ functions, blood coagulation profile, and ex vivo analyses of normal intestinal (and bone marrow) progenitor cell growth. Through extensive in vitro, in vivo, and ex vivo mechanistic studies, we showed that G2.2's inhibition of CSC self-renewal was mediated through activation of p38 α, uncovering important signaling that can be targeted to deplete CSCs selectively while minimizing host toxicity. Hence, G2.2 represents a first-in-class (NSGM) anti-cancer agent to reduce colorectal CSCs.

[*]Address for correspondence: 1) Bhaumik B Patel. 1201 Broad rock Blvd. Richmond, VA 23249. Phone: 804-675-5000 × 4310. Bhaumik.patel@vcuhealth.org. 2) Umesh R.Desai. 800 E. Leigh St. #212, Richmond, VA 23219. Phone: 804-828-7328. urdesai@vcu.edu.

Keywords

Cancer stem cells; Intestinal stem cells; Glycosaminoglycans; Glycosaminoglycan mimetics; Colon cancer; anti-cancer therapy

Introduction

Stem cells show a remarkable ability to self-renew and differentiate and replenish cells of a particular tissue that are lost as part of the natural processes or due to injury (1). Accumulating evidence suggests that colorectal cancers (CRCs) arise as a result of accumulating mutations in tissue-resident stem cells, which then transform into cancer stem cells (CSCs) (2). Hence, many of the self-renewal signaling pathways, e.g., Wnt-βcatenin-TCF4 signaling, are shared between NSCs and CSCs (3). Increasing evidence points to a critical role of CSCs in driving cancer metastasis, resistance to chemotherapy, and relapse following complete tumor resections leading to poor clinical outcomes (4). As a result, intensive efforts are being directed at discovering therapies that selectively target CSCs. Most such therapies have focused on targeting one of the transcriptional signaling that regulates CSC self-renewal, e.g., βcatenin, SHH, etc. Given the redundancy in the regulatory network of CSCs, the approach may have limited success while also raising concerns for toxicity to normal stem cells due to a shared transcriptional mechanism of self-renewal (5). Hence, there is an urgent need to identify upstream pathways that differentially regulate CSCs and normal stem cell growth. Likewise, agents that modulate these pathways to effect selective targeting of CSCs are also critically needed.

Arguably, microenvironmental components that serve as the stem cell niche have shown key differences with respect to NSCs and CSCs in many instances (6,7). Amongst the many cellular and molecular components of the microenvironment, glycosaminoglycans (GAGs) have emerged as essential regulators of stemness (8). GAGs, which are part of the cell surface macromolecules called proteoglycans, have been found to induce precise and coordinated modulation of key growth factors, cytokines and morphogens resulting in selective mitogen-activated protein kinases (MAPK) and/or another intracellular signaling (9). This in turn is known to regulate self-renewal (10,11). In fact, we recently demonstrated that a heparan sulfate (HS) sequence that is hexasaccharide (HS06) in length, but neither longer nor shorter than that, inhibits CSC self-renewal by isoform-specific activation of p38 MAPK (11). Interestingly, p38 MAPK was recently shown to promote differentiation of intestinal NSCs (12). These results provide a clue that HS06, or its mimetics, which induce p38 activation could prove to be valuable as clinically viable anti-CSC agents.

For a long time, it has been hypothesized that GAGs would inhibit cancer (13,14). In fact, polymeric heparin and variants thereof, e.g., 2-O,3-O desulfated heparin (ODSH) as well as oligosaccharide mixture PI-88, have been examined in cancer treatment (15–18). Heparin, PI-88 and other GAGs are highly heterogeneous, which generates major barrier for target selectivity. Problems of selectivity also arise from the primarily electrostatic nature of their interactions with proteins, which disfavor hydrogen bonding and hydrophobic (van der Waals) interactions. We have shown that sulfated non-saccharide GAG mimetics (NSGMs),

which are fully synthetic and homogeneous, bind to GAG-binding proteins through electrostatic, hydrogen bonding and van der Waals forces, thereby exhibiting much higher target selectivity (19–21). NSGMs also offer several other key advantages over GAGs as viable anti-cancer agents. These include ease and scalability of synthesis, ease of monitoring homogeneity of drug dose, and inexpensive cost of large scale preparation. In fact, we recently discovered that an NSGM called G2.2, which selectively inhibits CSC self-renewal *in vitro* (22), is a structural mimetic of HS06 (23). Hence, we hypothesized that G2.2 can inhibit CSC self-renewal, but promote NSC differentiation, *in vivo* by inducing p38 MPAK activation.

We show here that G2.2 inhibited colon CSCs-induced xenografts that were further enriched in CSCs through prior treatment with oxaliplatin and 5-fluorouracil, the most commonly used CRC chemotherapy combination, in a dose-dependent fashion. G2.2-induced p38α/β MAPK was required for former's anti-CSC effects *in vitro* as well as *in vivo*. Moreover, G2.2 demonstrated no gross toxicities or vital organ damage and had minimal anti-coagulant effects. Overall, the studies indicate that activation of p38α/β MAPK might serve as a CSCs-suppressive signaling and G2.2, an activator of p38α/β MAPK, represents a novel selective anti-CSC therapy with a significant translational potential.

Materials and Method

Chemicals

Reagents: Synthesis of G2.2 (purity 99%) was performed as described earlier (22). SB203580 (Selleckchem, Houston, TX) (24), as well as 5-Flurouracil, oxaliplatin, Tween 80, Dimethyl sulfoxide, and PEG300 (Sigma Aldrich) were purchased from commercial vendors.

Cell culture—Human colorectal (HT29 and HCT116) and pancreatic (Panc-1) cells were obtained from ATCC (Manassas, VA). MDA-MB-231 cell line was gift from Dr. Kolblinski (Virginia Commonwealth University). The cells were passaged as monolayers (11, 22, 24) for no more than six passages. The cells were tested for mycoplasma with the kit (ATCC 30–1012K) and disinfected with MPbio (San Diego) catalog # 093050044 within last 12 months. HT29 cells were transfected using mammalian p38α (Dharmacon # M-003512–02-0005) smart pool as well individual p38α siRNA (Dharmacon # D-003512–15 and D-003512–19) (25nM final concentration) with dharmafect duo reagent in a 6-well plate using manufacture's transfection protocol and plated for spheroid assay 48hr later.

Animal models: All experiments involving animals were approved by the Animal Component of Research Protocol Committee at Richmond VAMC.

Xenografts were generated by injecting 10^5 CD133 hi/CXCR4 hi (Dual hi) fluorescence-activated cell sorter (FACS) isolated HT-29/HCT 116 cells suspended in 50% reduced growth factor Matrigel (BD Bioscience) (in 50 μL sterile PBS) into the right flank of 6-week-old, female NCr nude mice (Taconic Farms, Germantown, NY) subcutaneously (s.c.). Once the average tumor volume reached 25–50 mm^3 (~day 13), animals were randomly assigned to respective treatments for the defined time.

Limiting dilution studies: In each group (N=16), were injected with 2,000 – 100,000 (N=4 mice/cell concentration) of CD133+/CXCR4+ (Dual hi) cells from HCT 116 or HT-29 subcutaneously (s.c.). The animals were then observed for the presence of palpable tumors >150mm^3.

Dose finding studies-: groups of animals N=8/group were injected intraperitoneal (i.p.) with 200μL saline or G2.2 (10→200 mg/kg) × 3 times a week for 5 weeks. Following treatment, mice were sacrificed at day 43 (one week after the last injection) and xenografts used for ex vivo CSC phenotype studies.

Secondary Xenograft studies-: Xenografts excised from mice treated with 100mg/Kg were finely chopped and digested as described below. Single cell suspension was obtained and 10^6 cells were injected s.c.. Once palpable tumors were observed these were randomized (N=5) to receive intraperitoneal (i.p.) injections of 200μL saline or G2.2 (100 mg/kg) × 3 times a week for 3weeks.

HCT 116 Xenograft studies-: Mice were injected with 10^5 Dual hi cells as described above. Groups of animals N=5/group were injected intraperitoneal (i.p.) with 200μL saline or G2.2 (175 mg/kg) × 3 times a week for 3 weeks. Following treatment, mice were sacrificed an hour after the final injection and xenografts used for ex vivo CSC phenotype studies.

Chemotherapy-enriched CSC xenograft model-: In the first phase, a group of 6-week-old, female NCr nude mice were randomized to vehicle (N=10) or FUOX (5-FU 25mg/kg and oxaliplatin 2mg/kg weekly) (n=17) for 3-weeks followed by the second randomization of FUOX treated animals (D-21 of initiation of FUOX) to vehicle (n=7) or G2.2 (200 mg/kg three times a week × 5 weeks) (n=7). Mice were euthanized at 1. post chemotherapy (day 21) 2. Day 30 and 3. day 42 post completion of treatment (an hour after the final injection) and ex vivo CSC phenotype studies performed.

Mechanistic studies-: Animals were randomly assigned to four groups for mechanistic studies that were injected intraperitoneal (i.p.) 1. Vehicle (**Veh**) 2. G2.2 (200mg/kg), 3. SB203580 (**SB**) (10mg/kg) and 4. (**SG**) SB, 3 hours prior to G2.2 (200 mg/kg) 3 times a week for 5 weeks. Following treatment (an hour after the final injection), mice were sacrificed and xenografts used for ex vivo CSC phenotype studies.

Tumor monitoring and euthanasia-: Tumor measurements were made three times a week with Vernier calipers, and tumor volume was calculated using the formula: $V = W^2 \times (L)/2$, where V=volume in mm^3, W and L= width and length in mm. At the end of the 5-weeks post treatment, appropriate number of animals were sacrificed in each group and the tumor tissue were collected and processed as below. The remainder of animals were monitored till they reached pre-defined humane end-points.

Preparation of animal tissues-

Animals were sacrificed per IACUC approved methods of euthanasia. The tumor tissue was finely chopped and digested with 400 μg/ml Collagenase Type IV (STEMCELL

Technologies, Vancouver, BC). Single cell suspension was filtered with 70μm cell strainer and used for one of the studies described below. The vital organs were harvested and fixed in 4% paraformaldehyde and sectioned using microtome. The slides stained with H&E and examined under light microscope.

Flow cytometry and Western-blot analyses

Flow cytometric analyses for CSC markers as well as western-blot analyses for CSC markers, self-renewal factors, and p38 MAPK was performed using methods described in earlier publications (11, 22, 24). The details of antibodies are provided in supplemental methods.

Colonosphere formation assay

Cells derived from xenografts as well as primary cells maintained as monolayer were plated in non-treated, low adhesion, 96 wells plates for 1/2/3/4 spheroids as described earlier (24).

Serum chemistry s

Serum chemistry was performed by the mouse phenotyping, physiology and metabolism core at the Penn diabetes research center located at the University of Pennsylvania health system.

Coagulation assay:

PT and aPTT were measured in plasma using standard one-stage clotting assays (STA PT-Neoplastin CI, STA PTT- Automate, respectively) on the STA Compact analyzer (Diagnostica Stago, Parsippany, NJ, USA) according to manufacturer's instructions.

Intestinal organoids

Mice intestinal pieces (2–4 cm) were subjected to chelation and dissociation into crypts using previously described methods (25). Approximately 200–500 crypts were then resuspended in 100μL of matrigel per well of a 96-well plate and overlayed with 100μL of IntestiCult™ Organoid Growth Medium (Mouse) (Stemcell technologies) after allowing for matrigel polymerization and cultured in the CO_2 incubator (37°C, 5% CO2). The intestinal organoids develop after 5–7 days of culturing.

The Mouse Colony Forming Cell (CFC) Assay

Briefly, a single cell suspension of mononuclear cells from mouse bone marrow was prepared to obtain ~2–4 × 10^7 hematopoietic cells using previous described methods (26). The cells were resuspended in 10mL of Iscove's modified Dulbecco's medium (IMDM/2% FBS media) (Allcells) and mixed with Methyl cellulose (R&D systems), and 1.1mL of the final cell mixture was added to a non-treated 6-well plate using a 3mL syringe. Water was added to one of the wells of the 6-well plate to maintain humidity necessary for colony development. Plates were incubated for 8–12 days at 37°C and 5% CO_2. Colonies consisting of at least 30 cells were counted.

Results

Dual hi (CD133+/CXCR4+) cells represent colon CSCs –

A high percentage of CD133+/CXCR4+ (Dual hi) in primary human primary CRC was associated with a poor prognosis (25). Earlier, we observed significantly increased spheroid formation using fluorescence activated cell sorted (FACS) Dual hi HT-29 cells compared to Dual lo (CD133-/CXCR4-) controls (26), suggesting enrichment of CSC population. Furthermore, magnetic-assisted cell sorting (MACS) experiments showed that only Dual hi but not CD133+/CXCR4-, CD133-/CXCR4+ HT-29 cells showed robust increase in 1° spheroid formation compared to Dual lo cells (Fig 1A). Indeed, Dual hi cells showed robust overexpression of not only CD133 and CXCR4, but also DCMKL1, LGR5, EpCAM, LRIG1 and NANOG mRNA (Fig 1B) and/or protein levels (Fig 1C), other bonafide makers of colon CSCs, compared to Dual lo controls in two colon cancer models - HT-29 (KRAS wt., P53 mut.) and HCT 116 (KRAS mut., and p53 wt.) that differ in common CRC genetic variant status. However, an accurate measure of CSCs can only be judged through in vivo limiting dilution assay. Indeed, both HT-29 and HCT 116 cells showed tumor formation (size >150 mm^3) in ≥ 50% of the animals with as few as 2×10e3 cells (Fig 1D). On the other hand, a similar number of Dual lo cells failed to form any tumor with either of the cells for >35 days following injection (Fig S1a). As 10e5 Dual hi cells generated xenografts consistently (100%) and rapidly in both cell line models (Fig 1E and S1b), we used that cell dose for xenograft formation in the efficacy studies of G2.2 below.

G2.2 selectively inhibits CSC-induced colon cancer xenograft growth in a dose-dependent manner

— Selective targeting of CSCs is a paradigm-shifting approach. G2.2, an NSGM of HS06 (23), was identified earlier as a potent and selective CSC inhibitor using a novel *in vitro* tandem, dual screen strategy (22). Buoyed by this advancement, we embarked on the *in vivo* evaluation of its therapeutic potential. HT-29 xenografts were induced by injecting 10e5 Dual hi cells subcutaneous (*s.c.*) in a group of 20 NCr nude mice. Mice were randomized to either vehicle or one of the doses of G2.2 (25→200 mg/kg, 3×/week for 5 weeks) delivered intraperitoneally (*i.p.*) after palpable tumors formed. We observed a dose-dependent inhibition of tumor volume in G2.2-treated animals compared to vehicle controls with maximal potency observed at doses of 200 mg/kg (Fig. 2A, Fig S2a) without any gross toxic effects (see toxicity studies below). The tumor volumes at day 43 displayed a robust >75% decrease in the G2.2 (200 mg/kg)-treated mice compared to vehicle controls (Fig. 2A) resulting in significantly improved survival using humane endpoint criteria (Fig S2a). Using 200 mg/kg of G2.2 as an optimal dose, we performed additional studies to understand its effect on CSCs growth better. Comparable to significant tumor volume changes, we observed a robust reduction in a complement of CSC markers (CD133, DCLK1, LRIG1, and LGR5) as well as self-renewal factor (BMI-1) (Fig 2B). Similarly, there was approximately 5-fold and 3.5-fold reduction in the numbers of $LGR5^+$ and Dual hi cells, respectively, in G2.2-treated xenografts compared to vehicle control (Fig. 2C, Fig S2b). Indeed, a similar reduction (4.5-fold) in Dual hi cells was also observed in HT-29 spheroids treated with G2.2 (100 μM) (Fig S2b), confirming inhibition of Dual hi CSCs by G2.2 in vitro and in vivo. We utilized our earlier observation that CSCs/progenitors are enhanced several-fold in spheroid

culture and assessed the xenografts-derived cells for retention of 2°→4° spheroid growth inhibition profiles to distinguish between non-self-renewing progenitors and self-renewing CSCs *ex-vivo*. (22,27) Indeed, cells derived from G2.2-treated xenografts showed a robust 7-fold decrease in 2°→4° spheroid formation, measured a week (Day 43) after the last dose of G2.2, compared to vehicle controls (Fig. 2D, Fig S2c). More importantly, akin to our *in vitro* studies,(22) we observed a robust induction of apoptosis in G2.2 treated xenografts compared to vehicle controls (Fig S2d), which was mainly restricted to Dual hi (50%) compartment with a minor effect in Dual lo (10%) compartment, suggesting selective targeting of CSCs in vivo by G2.2 (Fig. 2E, Fig S2d). Hence, G2.2 seems to be a first of its kind, novel NSGM that inhibits tumor growth by CSCs inhibition-dependent mechanism *in vivo*.

Despite robust growth inhibition of HT-29 xenograft by G2.2, residual tumors remain (Fig 2A). It is essential to determine if rapid resistance to therapy develops in vivo. We conducted additional studies on G2.2 sensitivity in residual G2.2-treated xenografts-derived cells in vitro (200 mg/kg cohort) and in vivo (100 mg/kg cohort). Post-G2.2 (200 mg/kg) treated xenograft-derived 3° spheroids were treated with G2.2 (100 μM) or vehicle and observed for 4° spheroids (presence of the drug) as well as 5° and 6° spheroids (absence of further G2.2 treatment). Indeed, G2.2 showed robust inhibition of 4°→6° spheroids (Fig S2d). Furthermore, G2.2 (100 mg/kg 3times/week × 3 weeks i.p.) showed potent inhibition of secondary xenografts (>50%) generated from post-G2.2 (100 mg/kg) treated xenografts-derived cells in NCr nude mice (Fig 2F) as well as ex vivo CSCs self-renewal (2°→4° spheroids) (Fig S2f) in cells derived from these secondary xenografts compared to respective vehicle-treated controls. Hence, G2.2 treatment does not induce rapid development of treatment resistance in vivo. Finally, G2.2 (175 mg/kg 3 times/week × 3 weeks i.p.) showed robust inhibition of another Dual hi-generated colon cancer xenograft (HCT 116) growth as well as ex vivo CSC phenotype (Figs 2G & S2g-h) as in HT-29 cells, suggesting likely generalizable effect of G2.2 on colon CSCs.

G2.2 inhibits CSCs in chemotherapy-enriched xenograft model

— Our subsequent study was designed to understand the efficacy of G2.2 in a CSC-enriched xenograft model. We utilized a dual enrichment strategy. In the first step, we performed *in vitro* enrichment, as described in the above model, by developing Dual hi HT29 cells-derived xenografts in nude mice. Combination of 5-fluorouracil and oxaliplatin (FUOX), which is the most frequently used chemotherapy for colon cancer, enriches CSCs *in vitro* (28). Hence, we performed a second step of CSC enrichment *in vivo*. This involved randomization of HT29 Dual Hi induced xenograft-bearing nude mice to *i.p.* administration of FUOX or vehicle weekly for 3 weeks. As expected, the dual enrichment strategy resulted in a further increase in the Dual hi cells as well as 2°→3° spheroids in chemotherapy-treated mice (11% *vs.* 6%) compared to vehicle controls (Figs. 3A & S3a-b). The overall lower CSC population in the xenograft (than at the time of original inoculation) can be attributed to the ability of CSCs to proliferate into non-CSC progenitor cells (29), as well as self-renew to maintain its own population in vivo post-inoculation. The chemotherapy-treated CSC enriched xenograft-bearing mice were then randomized (second randomization) to receive either G2.2 (200 mg/kg 3×/week × 10 injections i.p.) or vehicle. Hence, the study had three

groups including a) vehicle (Veh); b) chemotherapy followed by vehicle (CVeh) and b) chemotherapy followed by G2.2 (CG2.2). The results showed that there was 2-fold rapid increase in tumor volume in the CVeh mice compared to Veh (Fig 3A) accompanied by a progressive increase in Dual hi population (Fig 3C), which most probably arose from enhancement in CSC-mediated proliferation due to our dual enrichment strategy. More importantly, we observed a robust 7.6-fold ($p<0.01$) inhibition in tumor volume (day 30) (Fig 3A) resulting in improved survival using humane endpoint criteria (Fig 3B). The tumor volume changes were accompanied by a robust 4.3-fold reduction in the fraction of Dual hi cells (Fig 3D & S3c) as well as a complement of CSC makers/self-renewal factor (CD133, DCLK1, LRIG1, LGR5, BMI1) in CG2.2 xenografts compared to CVeh (Figs. 3C & S3d). Indeed, phenotypic CSC self-renewal studies with 2°→3° colonospheres (at both day 30 and 42 post-treatment initiation) showed a similar profile as the change in tumor volume, characterized by an increase in CVeh, but a robust decreased in CG2.2 treated animals compared to Veh controls (Figs. 3E & S3e). Overall, the data validate the in vivo efficacy of G2.2 in inhibiting chemotherapy-enriched CSC xenograft growth model.

G2.2 mimics HS06 to inhibit colon CSCs through activation of p38 MAPK

— As stated before, G2.2 is a structural mimetic of the natural HS06 sequence, as demonstrated in a recent study (23). We also reported that HS06 selectively inhibits CSC self-renewal through an isoform-specific activation of p38α MAPK (11). Thus, our expectation was that G2.2 would also induce activation of p38 MAPK. Indeed, like HS06, G2.2 induced early and sustained activation of p38 MAPK, but caused inhibition of ERK1/2 and JNK – the other related MAPK members (Fig S4a), in HT29 spheroids. Interestingly, inactive analogs of G2.2, G1.4, and G4.1, failed to activate p38 (Fig S4b) in HT29 spheroids. Measurement of phosphorylation level of p38 in colorectal (HCT116 & HT29), pancreatic (Panc-1) and breast (MDA-MB-231) cancer spheroids (enriched in CSCs) also revealed that G2.2 enhanced p38 activation nearly 1.5–2.7-fold. At the same time, p38 MAPK activation was not found in the corresponding monolayer counterparts (Fig. 4A), suggesting selectivity of G2.2 towards CSCs.

We performed immunoprecipitation with anti-pp38 antibody followed by western blotting with isoform-specific p38 antibodies following vehicle- or G2.2-treatment in HT29 spheroids to elucidate isoform specificity of p38 induction. G2.2 treatment resulted in activation of α and β isoforms (α > β), inhibition of the δ isoform, and no discernible effect on the γ isoform (Fig. S4c). The results indicated isoform-specific activation of p38 MAPK by G2.2. Importantly, pre-treatment with SB203580 (SB), a pharmacological inhibitor of p38α/β (24), mostly resulted in a near-complete reversal of G2.2-mediated inhibition of CSC self-renewal as evident in 3° spheroids formation (Fig 4B) as well as CSC markers (CD44, EPCAM) and self-renewal (BMI-1) factors (Fig. 4C). These results imply that p38α/β MAPK activation mediate the effects of G2.2 on CSC self-renewal. Furthermore, genetic depletion of p38α (siRNA) in HT-29 spheroids (Figs. 4D & S4d-e), as well as function p38α inhibition using a dominant-negative vector (p38α agf) in both HT-29 and HCT 116 spheroids (Figs 4E-F & S4f) produced results identical to SB203580. Overall, these findings point to a highly specific modulation of p38 MAPK in the regulation of CSCs self-renewal

by G2.2. Moreover, these findings are virtually identical to the effects observed with HS06 strongly implying functional mimicry of HS06 by G2.2 (11).

G2.2 inhibits colon CSCs *in vivo* through the p38 activation-dependent mechanism

— To test p38α/β activation-based anti-CSC mechanism of G2.2 *in vivo,* we performed mice xenograft experiments similar to that described in Figure 1 using G2.2 (inducer) and SB (inhibitor) as p38α/β modulators. Mice induced with 1×10^5 Dual Hi HT29 cell xenografts were randomized to *i.p.* administration of i) vehicle (Veh); ii) G2.2 (200 mg/kg); iii) SB (10 mg/kg) and iv) SB 3 hours prior to G2.2 (SG) three times a week for three weeks. As expected, G2.2 displayed a substantial decrease in tumor volume (4.6-fold) when compared to vehicle (Fig. 5A), which was also corroborated by a similar reduction in 3^O spheroids (Fig 5B), Dual hi CSC population (Fig. 5C), and levels of CSC markers (CD133, LGR5) and self-renewal (BMI1) factor (Fig 5D). Intriguingly, SB alone caused a modest decrease in tumor volume (Fig 5A). The latter observation can be attributed to a chemotherapy-like targeting of non-CSCs as we observed enrichment of Dual hi CSCs, increase in 2^O spheroids, and levels of CSC/self-renewal markers (Fig. 5B-D). Indeed, as observed in the *in vitro* studies, administration of SB followed by G2.2 (SG) produced near-complete reversal of G2.2's effect on tumor volume, 2^O spheroids, Dual hi population, and CSC/self-renewal makers (Fig. 5A-D & Fig S5a). Indeed, G2.2 caused activation, SB induced inhibition, and SG caused no change in levels of pp38 (the activated form of p38 MAPK) (Fig. 5D). These findings support the conclusion that activation of p38 α/β largely drives *in vivo* anti-CSC effects of G2.2.

G2.2 exhibits none to minimal untoward effects on critical organs or adult stem/progenitor cell function in nude mice

— Given the robust anti-CSC efficacy of G2.2 *in vivo*, we proceeded to elucidate the toxicity profile *in vivo* to assess its true therapeutic potential. The toxicity was determined at different levels including a) gross, b) vital organ damage and c) progenitor cell growth. We also studied its effect on coagulation as GAGs and NSGMs may inhibit coagulation enzymes (30,31). At a gross level, *i.p.* administration of G2.2 (200 mg/kg, 3times/week × 5 weeks) in the above studies did not produce any significant weight loss in mice (Fig S6a). Mice showed normal behavior with no external signs of distress, allergy-induced rashes, diarrhea, or significant deviation from expected repertoire throughout the course of the treatment. A thorough assessment of critical vital organ damage was conducted by measuring a) morphology (H&E) and b) serum chemistry in G2.2 and vehicle-treated mice. No significant changes in tissue morphology were observed in G2.2-, compared to vehicle-, treated mice organs (Fig 6A) except in the liver. The liver in G2.2-treated mice showed a minor ~5% dropout in hepatocytes (Fig S6b). However, serum chemistry revealed no significant alterations in various electrolyte levels or biomarkers indicating hepatic (e.g., Ast, Alt), renal (creatinine) and muscle damage (Cpk) (Fig. 6B). Hence, we conclude that the changes in the liver morphology are unlikely to be of any major clinical significance.

GAG's are known to interact with many proteins of the coagulation system. Hence, we studied the anticoagulation potential of G2.2 through APTT and PT studies, which are routinely used to assess the anticoagulation state of blood/plasma. The APTTs of plasma

collected from G2.2-compared to vehicle-treated mice were found to be substantially similar, while a modest delay in the extrinsic clotting time (PT) was observed for G2.2-treated plasma (Fig. 6C).

As CSCs and normal stem/progenitors (NSCs) utilize common pathways of self-renewal, it was essential to examine G2.2's effect on the NSCs. The NSC population in the bone marrow and the intestines are abundant and differentiate continuously to fulfill functions of blood cells while also replenishing the surface lining in the bone marrow and the intestines (32,33). We first examined the proportion of $LGR5^+$ cells in the colonic mucosa using flow-cytometry. Intriguingly, G2.2 had no discernible effects on the number of adult colonic NSCs (Fig. 6D). To further understand the effects of G2.2 on the proliferative function of NSCs, we examined *ex vivo* intestinal organoids and bone marrow colonies formation in G2.2- and vehicle-treated nude mice by harvesting the respective organs, as reported in the literature (34,35). Chronic administration of G2.2 (200 – 400 mg/kg) had none to a minimal inhibitory effect on small intestinal and colonic organoid ($1^O/2$) formation or bone marrow mixed colony formation compared to vehicle control (Fig. 6E). The results suggested no untoward effect on the function of the intestine and bone marrow NSCs/progenitors.

Thus overall, G2.2 exhibited minimal systemic effects in nude mice including preserving adult colonic/marrow NSC function while exhibiting potent anti-CSC effects towards colon CSCs. These findings support G2.2 as a potential therapeutic agent.

Discussion

GAGs have been known to play essential roles in several cancer-related processes including fine-tuning of growth factor receptor signaling, tumor angiogenesis, and metastasis (9,13,14). In fact, we recently presented evidence that a heparan sulfate hexasaccharide (HS06) sequence, but not any other longer or shorter sequence including UFH, LMWH, ODSH, and fondaparinux, has the unique ability to selectively inhibit CSCs from a variety of organ types (11). HS06 is particularly useful because it carries minimal anticoagulant potential as compared to UFH, LMWH, and fondaparinux. More importantly, the delicate chain length dependence of anti-CSC activity suggests finely tuned biology that may be amenable for therapeutic targeting.

Developing HS06 as an anti-CSC agent is challenging. HS06 synthesis or isolation from UFH is an incredibly painstaking as well as an expensive proposition. Instead, it might be advisable to develop HS06 mimetics that are easier to synthesize and purify. Hence, we resorted to the approach of studying NSGMs, which are not only easy to synthesize but also structurally homogeneous and likely to be more selective in protein recognition because of their hydrophobic aromatic scaffold. Hence, the discovery of G2.2, a structural mimetic of HS06 (23), as a robust and selective anti-CSC agent is a significant advancement in developing GAG-based anti-cancer agents. In fact, relapse following chemotherapy is generally attributed to the enrichment of CSCs post-chemotherapy (36,37). To this end, our studies provide the proof-of-the-concept that inhibition of CSCs is a viable strategy to halt tumor regrowth post-chemotherapy treatment.

Polymeric GAGs are known to interact with a plethora of proteins to regulate many pathophysiologic responses (14,38–43). G2.2 (1701 Da), in contrast, is much smaller and more homogenous than polymeric GAGs (15,000–50,000 Da). Despite these advantages, one could theoretically expect G2.2 to interact with several GAG-binding proteins in the manner of polymeric GAGs. Thus, G2.2's toxicity profile was essential to characterize. In combined morphological and biochemical studies of vital organ functions, G2.2 demonstrated excellent tolerance and lack of significant toxicity at anti-cancer doses. Concerning its anticoagulation profile, there was a modest increase in PT (INR < 2) but no significant effect on APTT with chronic administration of G2.2 at 200 mg/kg. Importantly, the latter was not associated with any major bleeding. Despite these positive results, it is important to note that toxicities studies were conducted in immunocompromised mice. It will be important to perform similar toxicity studies in immunocompetent mice in the future as GAGs are known to modulate immune function in vivo (44).

While G2.2 robustly inhibited cancerous intestinal stem cells, it has no apparent ill-effects towards normal intestinal stem cell function. This property of G2.2, selective targeting of CSCs, while sparing NSCs, is highly desirable in a selective anti-CSC agent. Often, the therapies that are developed to target CSCs, e.g., Wnt−β-catenin, notch, and hedgehog inhibitors, are likely to affect NSC function as many of these pathways are shared between CSCs and NSCs *albeit* with different degrees of dependence. In this respect, G2.2 is likely to be a unique agent. It appears to be inducing a common singling that differentially regulates CSCs and NSCs, thus providing a greater therapeutic window with respect to toxicity towards NSCs. Can p38 MAPK activation as the common signaling achieve such differential response? Although this question remains to be fully answered, the data discussed below support the latter hypothesis.

Mammalian p38 MAPKs are activated in the wide range of stimuli, ranging from physiological processes such as cell differentiation to pathological states including cancer. Activation of p38 MAPK has been shown to display often opposing, roles in different organs, cell types, and pathophysiologic conditions (10). In fact, the tumor suppressor role of p38α/β in various cancer has been reported. More recently, others and we have highlighted the importance of p38 activation in suppression of the CSC self-renewal (11,45). Intriguingly, recent reports support the role of p38 activation in promoting normal stem cell differentiation in the intestine (12) and/or bone marrow (46) has come to light. In the future, a differential role of G2.2 against CSCs and NSCs will have to be assessed in mice bearing murine colonic tumors using chemically-induced, or genetic models of colon cancer. In fact, such studies should ideally be performed in LGR5 reporter mice as one will be able to visualize the effect of the molecule on both CSCs and NSCs.

In conclusion, our studies offer a paradigm-shifting approach of selectively targeting CSCs to prevent tumor regrowth following traditional chemotherapy that often enriches CSCs. Additionally, our mechanistic studies bring to the light importance of p38α/β signaling as a therapeutic target to achieve a degree of selectivity towards CSCs. Moreover, G2.2's highly selective phenotypic properties bode well for NSGM technology to deliver additional promising therapeutic agents for cancer and other pathophysiologic conditions where GAGs play a key role.

Supplementary Material

Refer to Web version on PubMed Central for supplementary material.

Acknowledgement:

This work was supported in part by Veteran Affairs Merit Award 5I01BX000837 awarded to B.B. Patel, National Heart, Lung and Blood grants HL107152, HL090586 and HL128639 awarded to U.R. Desai, and Massey Cancer Center Pilot Project Fund A35365 B.B. Patel and U.R. Desai. We also thank the computing resources made available through the S10RR027411 grant from the National Center for Research Resources to Virginia Commonwealth University. Services and products in support of the research project were generated by the VCU Massey Cancer Center Flow Cytometry Shared Resource and Cancer Mouse Model Shared Resource, supported, in part, with funding from NIH-NCI Cancer Center Support Grant P30 CA016059. Service and products for research were also generated by Penn diabetes research center grant P30-DK19525 metabolism core.

Financial information/ Conflict of interest statement: “The authors have declared that no conflict of interest exists.”

References:

1. Jordan CT, Guzman ML, Noble M. Cancer stem cells. N Engl J Med 2006;355:1253–61 [PubMed: 16990388]
2. Rich JN. Cancer stem cells: understanding tumor hierarchy and heterogeneity. Medicine (Baltimore) 2016;95:S2–7 [PubMed: 27611934]
3. Yoo YD, Kwon YT. Molecular mechanisms controlling asymmetric and symmetric self-renewal of cancer stem cells. J Anal Sci Technol 2015;6:28 [PubMed: 26495157]
4. Clarke MF, Dick JE, Dirks PB, Eaves CJ, Jamieson CH, Jones DL, et al. Cancer stem cells--perspectives on current status and future directions: AACR Workshop on cancer stem cells. Cancer Res 2006;66:9339–44 [PubMed: 16990346]
5. Reya T, Morrison SJ, Clarke MF, Weissman IL. Stem cells, cancer, and cancer stem cells. Nature 2001;414:105–11 [PubMed: 11689955]
6. Tan DW, Barker N. Intestinal stem cells and their defining niche. Curr Top Dev Biol 2014;107:77–107 [PubMed: 24439803]
7. Plaks V, Kong N, Werb Z. The cancer stem cell niche: how essential is the niche in regulating stemness of tumor cells? Cell Stem Cell 2015;16:225–38 [PubMed: 25748930]
8. Klim JR, Li L, Wrighton PJ, Piekarczyk MS, Kiessling LL. A defined glycosaminoglycan-binding substratum for human pluripotent stem cells. Nat Methods 2010;7:989–94 [PubMed: 21076418]
9. Shute J Glycosaminoglycan and chemokine/growth factor interactions. Handb Exp Pharmacol 2012:307–24
10. Oeztuerk-Winder F, Ventura JJ. The many faces of p38 mitogen-activated protein kinase in progenitor/stem cell differentiation. Biochem J 2012;445:1–10 [PubMed: 22702973]
11. Patel NJ, Sharon C, Baranwal S, Boothello RS, Desai UR, Patel BB. Heparan sulfate hexasaccharide selectively inhibits cancer stem cells self-renewal by activating p38 MAP kinase. Oncotarget 2016;7:84608–22 [PubMed: 27705927]
12. Rodriguez-Colman MJ, Schewe M, Meerlo M, Stigter E, Gerrits J, Pras-Raves M, et al. Interplay between metabolic identities in the intestinal crypt supports stem cell function. Nature 2017;543:424–7 [PubMed: 28273069]
13. Yip GW, Smollich M, Gotte M. Therapeutic value of glycosaminoglycans in cancer. Mol Cancer Ther 2006;5:2139–48 [PubMed: 16985046]
14. Sasisekharan R, Shriver Z, Venkataraman G, Narayanasami U. Roles of heparan-sulphate glycosaminoglycans in cancer. Nat Rev Cancer 2002;2:521–8 [PubMed: 12094238]
15. Macbeth F, Noble S, Evans J, Ahmed S, Cohen D, Hood K, et al. Randomized Phase III Trial of Standard Therapy Plus Low Molecular Weight Heparin in Patients With Lung Cancer: FRAGMATIC Trial. J Clin Oncol 2016;34:488–94 [PubMed: 26700124]

16. van Doormaal FF, Di Nisio M, Otten HM, Richel DJ, Prins M, Buller HR. Randomized trial of the effect of the low molecular weight heparin nadroparin on survival in patients with cancer. J Clin Oncol 2011;29:2071–6 [PubMed: 21502549]
17. Zhang N, Lou W, Ji F, Qiu L, Tsang BK, Di W. Low molecular weight heparin and cancer survival: clinical trials and experimental mechanisms. J Cancer Res Clin Oncol 2016;142:1807–16 [PubMed: 26912316]
18. Liu CJ, Chang J, Lee PH, Lin DY, Wu CC, Jeng LB, et al. Adjuvant heparanase inhibitor PI-88 therapy for hepatocellular carcinoma recurrence. World J Gastroenterol 2014;20:11384–93 [PubMed: 25170226]
19. Mehta AY, Desai UR. Substantial non-electrostatic forces are needed to induce allosteric disruption of thrombin's active site through exosite 2. Biochem Biophys Res Commun 2014;452:813–6 [PubMed: 25201728]
20. Desai UR. The promise of sulfated synthetic small molecules as modulators of glycosaminoglycan function. Future Med Chem 2013;5:1363–6 [PubMed: 23919545]
21. Afosah DK, Al-Horani RA, Sankaranarayanan NV, Desai UR. Potent, Selective, Allosteric Inhibition of Human Plasmin by Sulfated Non-Saccharide Glycosaminoglycan Mimetics. J Med Chem 2017;60:641–57 [PubMed: 27976897]
22. Patel NJ, Karuturi R, Al-Horani RA, Baranwal S, Patel J, Desai UR, et al. Synthetic, non-saccharide, glycosaminoglycan mimetics selectively target colon cancer stem cells. ACS Chem Biol 2014;9:1826–33 [PubMed: 24968014]
23. Nagarajan B, Sankaranarayanan NV, Patel BB, Desai UR. A molecular dynamics-based algorithm for evaluating the glycosaminoglycan mimicking potential of synthetic, homogenous, sulfated small molecules. PLoS One 2017;12:e0171619 [PubMed: 28182755]
24. Low JL, Jurjens G, Seayad J, Seow J, Ting S, Laco F, et al. Tri-substituted imidazole analogues of SB203580 as inducers for cardiomyogenesis of human embryonic stem cells. Bioorg Med Chem Lett 2013;23:3300–3 [PubMed: 23602399]
25. Zhang SS, Han ZP, Jing YY, Tao SF, Li TJ, Wang H, et al. CD133(+)CXCR4(+) colon cancer cells exhibit metastatic potential and predict poor prognosis of patients. BMC Med 2012;10:85 [PubMed: 22871210]
26. Sharon C, Baranwal S, Patel NJ, Rodriguez-Agudo D, Pandak WM, Majumdar AP, et al. Inhibition of insulin-like growth factor receptor/AKT/mammalian target of rapamycin axis targets colorectal cancer stem cells by attenuating mevalonate-isoprenoid pathway in vitro and in vivo. Oncotarget 2015;6:15332–47 [PubMed: 25895029]
27. Patel N, Baranwal S, Patel BB. A strategic approach to identification of selective inhibitors of cancer stem cells. Methods Mol Biol 2015;1229:529–41 [PubMed: 25325978]
28. Patel BB, Gupta D, Elliott AA, Sengupta V, Yu Y, Majumdar AP. Curcumin targets FOLFOX-surviving colon cancer cells via inhibition of EGFRs and IGF-1R. Anticancer Res 2010;30:319–25 [PubMed: 20332435]
29. Tang DG. Understanding cancer stem cell heterogeneity and plasticity. Cell Res 2012;22:457–72 [PubMed: 22357481]
30. Senzolo M, Coppell J, Cholongitas E, Riddell A, Triantos CK, Perry D, et al. The effects of glycosaminoglycans on coagulation: a thromboelastographic study. Blood Coagul Fibrinolysis 2007;18:227–36 [PubMed: 17413758]
31. Mehta AY, Mohammed BM, Martin EJ, Brophy DF, Gailani D, Desai UR. Allosterism-based simultaneous, dual anticoagulant and antiplatelet action: allosteric inhibitor targeting the glycoprotein Ibalpha-binding and heparin-binding site of thrombin. J Thromb Haemost 2016;14:828–38 [PubMed: 26748875]
32. Eaves CJ. Hematopoietic stem cells: concepts, definitions, and the new reality. Blood 2015;125:2605–13 [PubMed: 25762175]
33. Barker N Adult intestinal stem cells: critical drivers of epithelial homeostasis and regeneration. Nat Rev Mol Cell Biol 2014;15:19–33 [PubMed: 24326621]
34. O'Rourke KP, Ackerman S, Dow LE, Lowe SW. Isolation, Culture, and Maintenance of Mouse Intestinal Stem Cells. Bio Protoc 2016;6

35. Fortier AH, Falk LA. Isolation of murine macrophages. Curr Protoc Immunol 2001;Chapter 14:Unit 14 1

36. Sosa MS, Bragado P, Aguirre-Ghiso JA. Mechanisms of disseminated cancer cell dormancy: an awakening field. Nat Rev Cancer 2014;14:611–22 [PubMed: 25118602]

37. Shi Q, Andre T, Grothey A, Yothers G, Hamilton SR, Bot BM, et al. Comparison of outcomes after fluorouracil-based adjuvant therapy for stages II and III colon cancer between 1978 to 1995 and 1996 to 2007: evidence of stage migration from the ACCENT database. J Clin Oncol 2013;31:3656–63 [PubMed: 23980089]

38. Lindahl U Heparan sulfate-protein interactions--a concept for drug design? Thrombosis and haemostasis 2007;98:109–15 [PubMed: 17598000]

39. Dreyfuss JL, Regatieri CV, Jarrouge TR, Cavalheiro RP, Sampaio LO, Nader HB. Heparan sulfate proteoglycans: structure, protein interactions and cell signaling. An Acad Bras Cienc 2009;81:409–29 [PubMed: 19722012]

40. Chen G, Deng C, Li YP. TGF-beta and BMP signaling in osteoblast differentiation and bone formation. International journal of biological sciences 2012;8:272–88 [PubMed: 22298955]

41. Sharon C, Baranwal S, Patel NJ, Rodriguez-Agudo D, Pandak WM, Majumdar AP, et al. Inhibition of insulin-like growth factor receptor/AKT/mammalian target of rapamycin axis targets colorectal cancer stem cells by attenuating mevalonate-isoprenoid pathway in vitro and in vivo. Oncotarget 2015

42. Nautiyal J, Du J, Yu Y, Kanwar SS, Levi E, Majumdar AP. EGFR regulation of colon cancer stem-like cells during aging and in response to the colonic carcinogen dimethylhydrazine. Am J Physiol Gastrointest Liver Physiol 2012;302:G655–63 [PubMed: 22281474]

43. Herreros-Villanueva M, Zubia-Olascoaga A, Bujanda L. c-Met in pancreatic cancer stem cells: therapeutic implications. World journal of gastroenterology : WJG 2012;18:5321–3 [PubMed: 23082047]

44. Simon Davis DA, Parish CR. Heparan sulfate: a ubiquitous glycosaminoglycan with multiple roles in immunity. Front Immunol 2013;4:470 [PubMed: 24391644]

45. Yang Y, Li Y, Wang K, Wang Y, Yin W, Li L. P38/NF-kappaB/snail pathway is involved in caffeic acid-induced inhibition of cancer stem cells-like properties and migratory capacity in malignant human keratinocyte. PLoS One 2013;8:e58915 [PubMed: 23516577]

46. Chang J, Sonoyama W, Wang Z, Jin Q, Zhang C, Krebsbach PH, et al. Noncanonical Wnt-4 signaling enhances bone regeneration of mesenchymal stem cells in craniofacial defects through activation of p38 MAPK. J Biol Chem 2007;282:30938–48. [PubMed: 17720811]

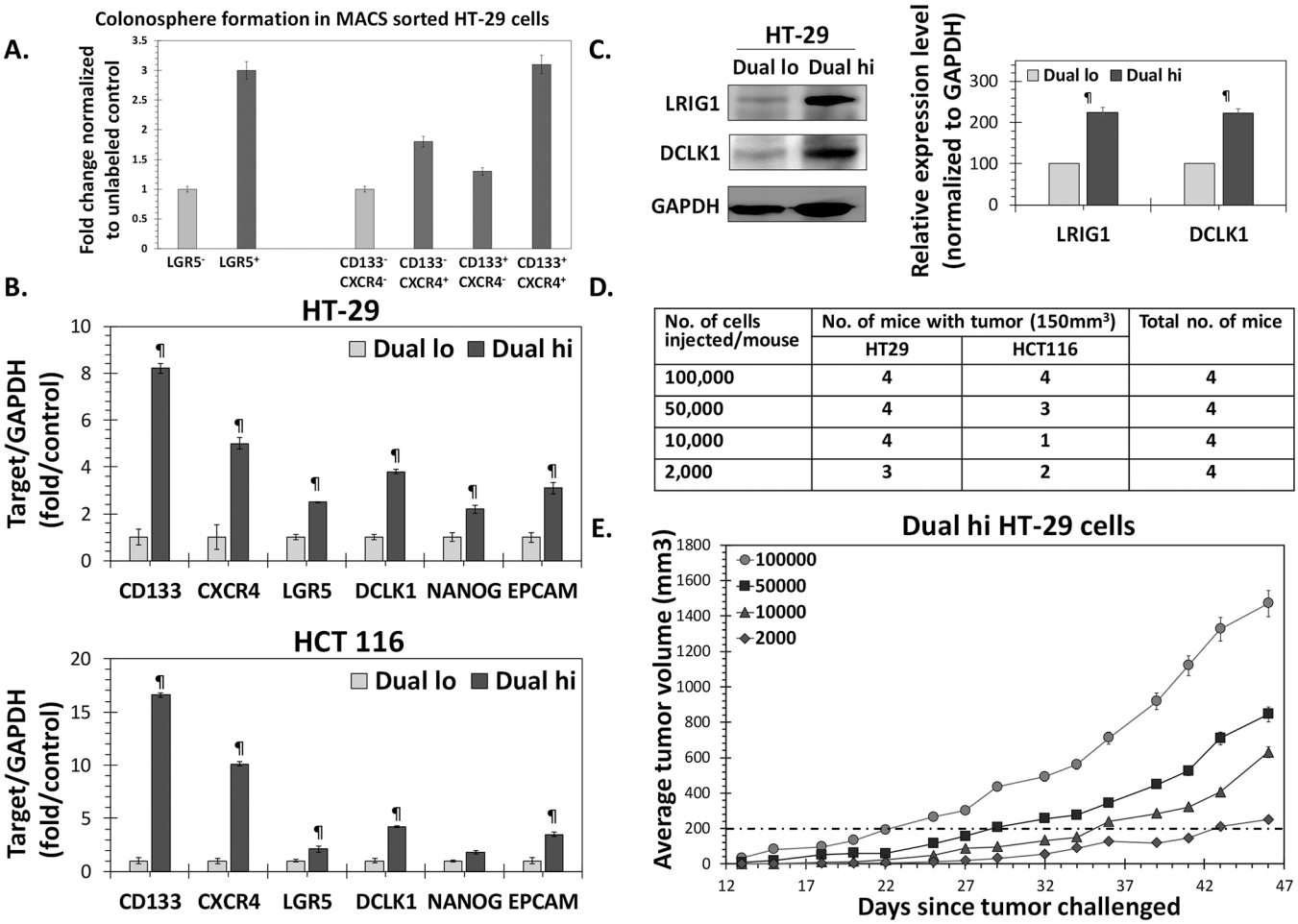

No. of cells injected/mouse	No. of mice with tumor (150mm³)		Total no. of mice
	HT29	HCT116	
100,000	4	4	4
50,000	4	3	4
10,000	4	1	4
2,000	3	2	4

Figure 1: Dual hi (CD133+/CXCR4+) cells represent colon CSCs.

(**A**) Primary colonosphere formation in MACS sorted HT-29 Dual hi vs. Dual lo, CD133+/CXCR4-, and CD133-/CXCR4+; as well as LGR5+ vs. LGR5- cells. (**B**) Q-PCR analyses demonstrating increased expression of other CSC markers (DCLK1, LGR5, EPCAM) /self-renewal factor (NANOG) in FACS sorted HT-29 and HCT 116 Dual hi compared to Dual lo controls. Data was normalized to GAPDH (housekeeping gene). (**C**) Western blot analyses of FACS sorted HT-29 cells shows higher expression of CSC makers (LRIG1, DCLK1) in Dual hi compared to Dual lo cells. The associated bar-graph represents relative densitometry value normalized to GAPDH (housekeeping protein). (**D**) In vivo limiting dilution assay to determine tumor formaing frequency with 10e5→2×10e3 Dual hi HT-29 and HCT 116 cells in athymic NCr nude mice. (**E**) Tumor growth profiles of 10e5→2×10e3 Dual hi HT-29 cells injected s.c.

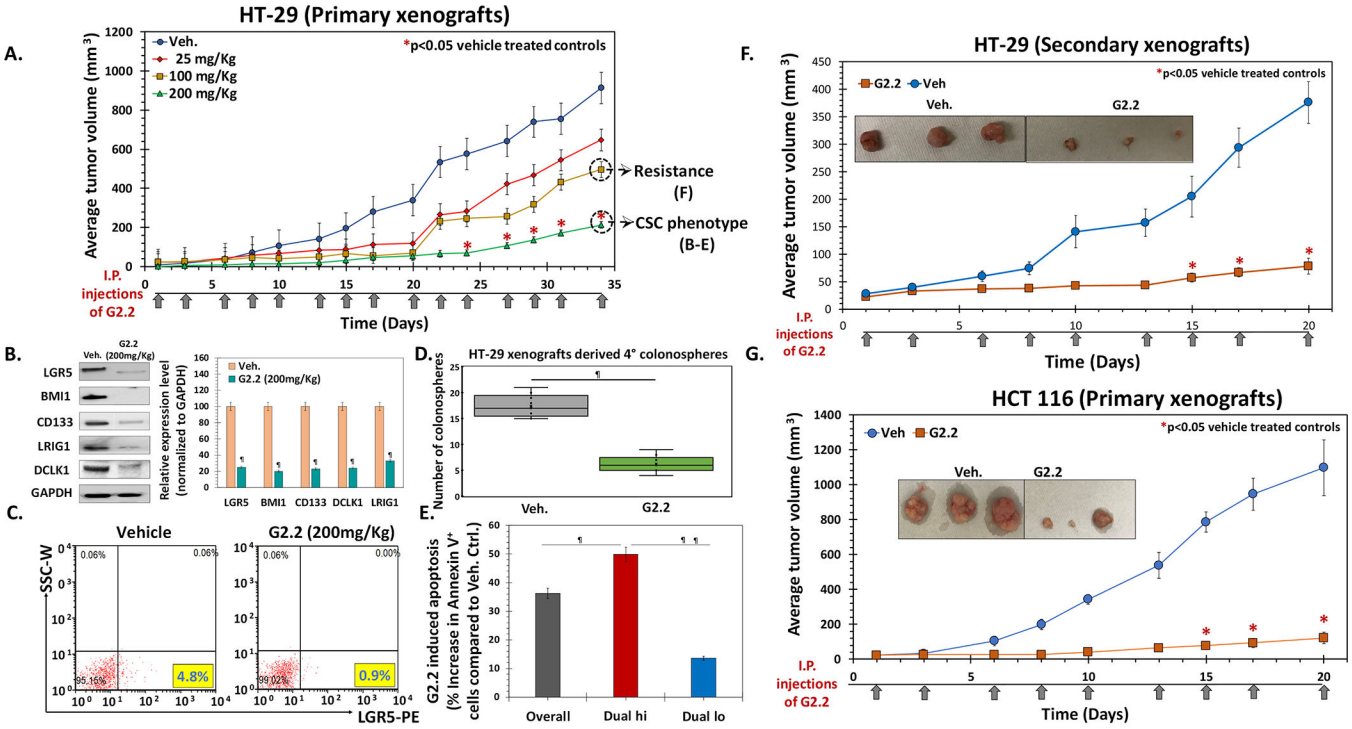

Figure 2: G2.2 selectively inhibits CSC-induced colon cancer xenograft growth in a dose dependent manner.

(**A**) G2.2 displays a dose dependent decrease in tumor volumes (25→200 mg/kg, 3×/week for 5 weeks). 10e5 Dual hi HT-29 cells were injected s.c. to generate xenografts. (**B**) Western blot analyses of xenografts show robust inhibition of CSC makers (LGR5, CD133, DCLK1, LRIG1) and self renewal factor (BMI1) in G2.2 treated xenografts compared to vehicle controls at day 43 post treatment initiation. The associated bar-graph represents relative densitometry value normalized to GAPDH (housekeeping protein). (**C**) Flow cytometry analyses of xenograft-derived cells labelled with anti-LGR5-PE antibody demonstrating robust inhibition of CSCs in G2.2 treated mice compared to vehicle controls. (**D**) G2.2 treated xenograft-derived cells show significant inhibition of CSC self-renewal (4° sphere formation) compared to vehicle controls. (**E**) Bar graph reperesentation of flow-cytometric analyses of apoptotic cells (annexin-V+) in Dual hi (CD133+/CXCR4+) CSCs as well as Dual lo non-CSCs populations in G2.2-treated (200 mg/kg) xenograft-derived cells. (**F**) G2.2 (100 mg/kg, 3 times/wk × 3 weeks) treatment showed continued inhibition of secondry xenografts generated from residual G2.2-treated (100 mg/kg, 3 times/week × 5 wks.) xenograft-derived cells in NCr nude mice, suggesting lack of rapid development of resistance to G2.2 in vivo. (**G**) G2.2 (200 mg/kg, 3 times/week × 3 wks.) also displays a robust decrease in 10e5 Dual hi HCT 116 cells induced xenografts in NCr nude mice. Panel inserts within the growth curves (panels F & G) show photomicrographs of representative xenografts at the end of 3 weeks treatment with G2.2. The arrows under each growth curves represent G2.2 treatment. Error bars represent ±1 SEM. * p-value < 0.05 compared to vehicle control, ¶ p-value <0.005 compared to vehicle control.

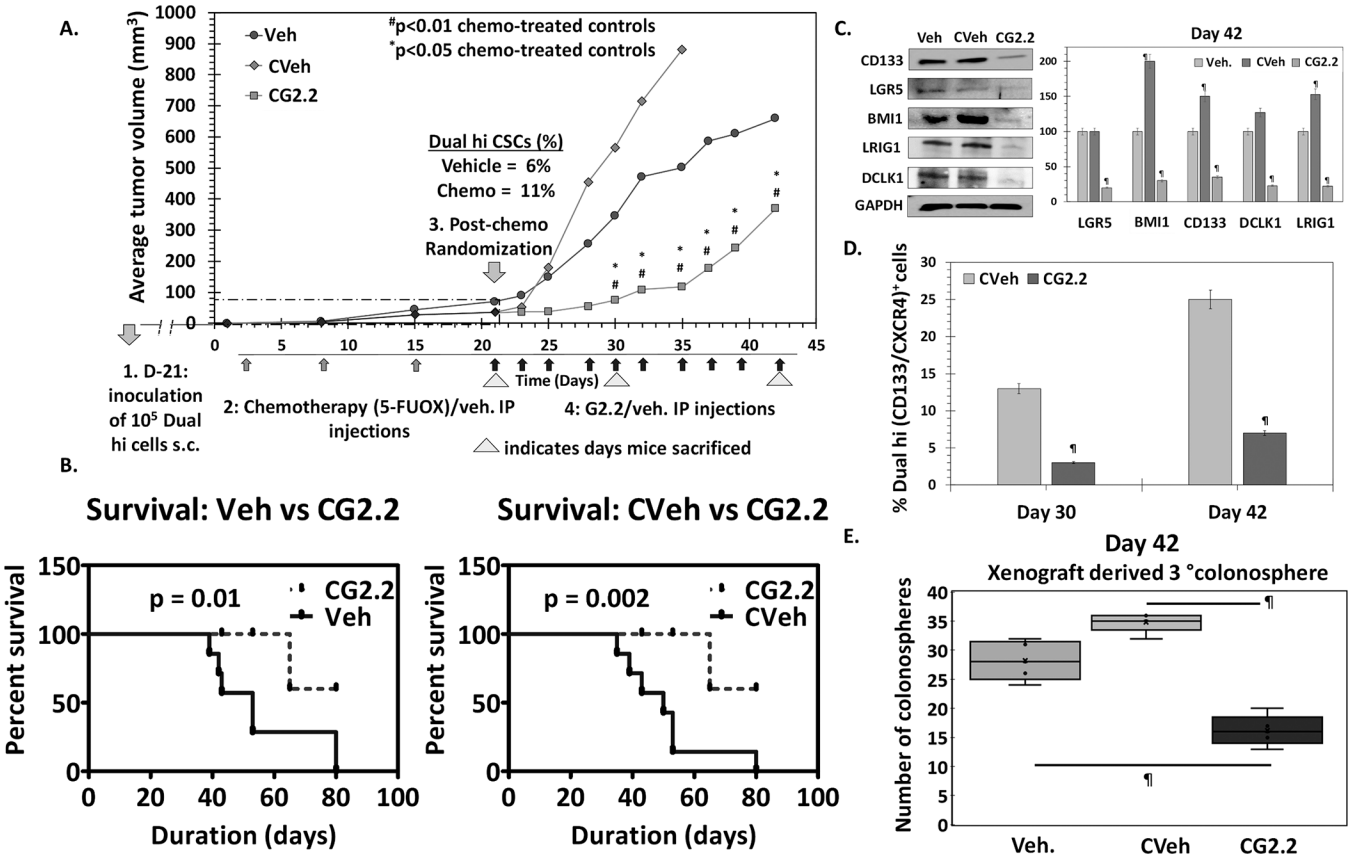

Figure 3: G2.2 inhibits CSCs in chemotherapy-enriched xenograft model.

(A) 5-flurouracil (25mg/kg) and oxaliplatin (2mg/kg) (FUOX) treatment (weekly × 3 weeks i.p.) of HT-29 Dual hi induced xenograft caused a modest reduction in tumor volume but significant enrichment of Dual hi CSCs. Treatment with G2.2 (200mg/kg 3 times/week × 10 injections i.p.) introduced at day 21 post-FUOX treatment-initiation produced significant reduction in tumor volume compared to Veh and CVeh. The arrows under the growth curves represent G2.2 treatment. **(B)** Bar graph representation of the flow cytometric analyses to determine proportion of Dual hi cells show significant reduction of CSCs by CG2.2 compared to CVeh. (**C**) FUOX treated xenograft-derived cells (CVeh) showed significant increase in CSC self-renewal (4° sphere formation) which was promptly inhibited by CG2.2 compared to both Veh. and CVeh treatments. **(D)** Western blot analyses and the corresponding bar graphs showing relative densitometric values normalized to GAPDH demonstrate inhibition of CSC (LGR5, CD133, LRIG1, DCLK1) and self renewal (BMI1) markers compared to both Veh and CVeh controls. Of note, CVeh xenograft showed incresed expression of CSC/self-renewal markers compared to Veh controls. (**E**) CG2.2 treated xenograft-derived cells show significant inhibition of CSC self-renewal (3° sphere formation) compared to both Cveh and Veh controls. Error bars represent ±1 SEM. #p-value < 0.01 compared to CVeh treated control and *p value <0.05 compared to Veh treated control. ¶p-value < 0.005 compared to Veh treated control.

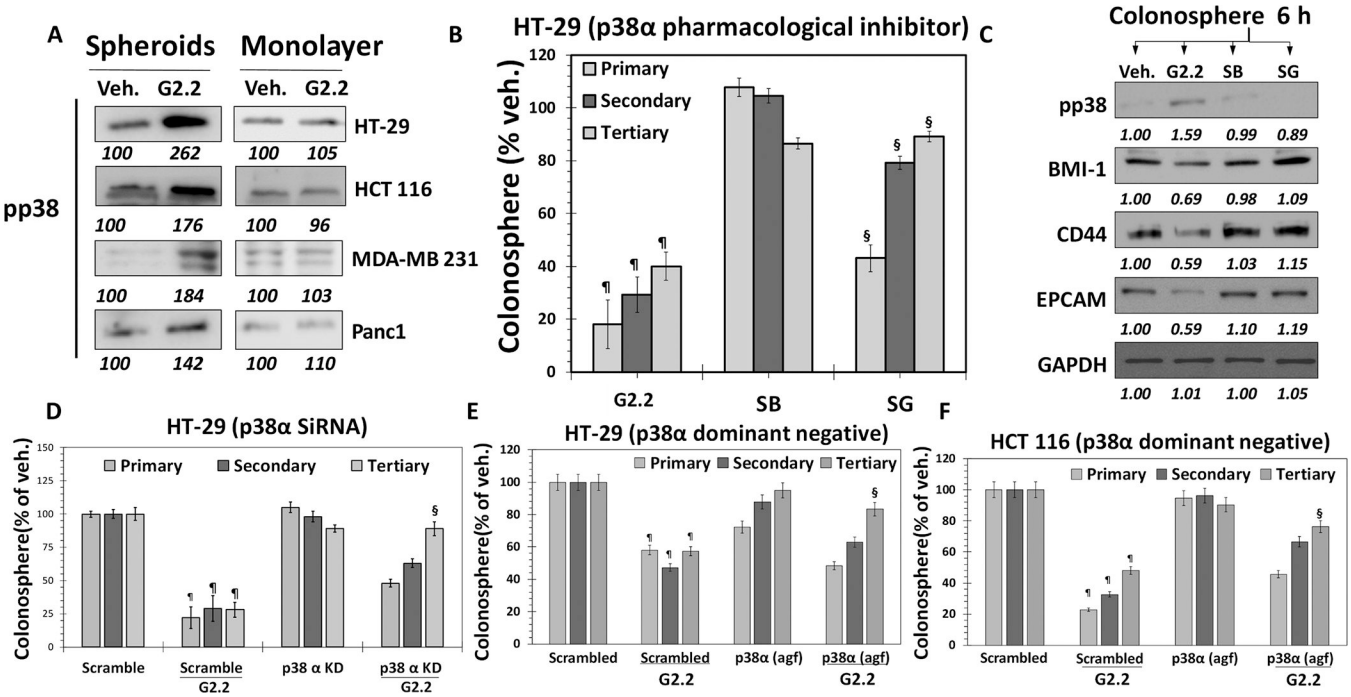

Figure 4: G2.2 mimics HS06 to inhibit colon CSCs through activation of p38 MAPK.

(A) Western blot analyses indicating increased pp38 levels in G2.2 treated colon (HT-29 and HCT 116), Breast (MDA-MB-231) and pancreatic (Panc1) spheroids but not in their monolayer counterparts compared to Veh. controls indicating selective induction of pp38 in CSCs. **(B & C)** G2.2 (100 μM) induced inhibition of HT-29 CSC self-renewal (3° sphere formation) and CSC (CD44, EPCAM)/self-renewal (BMI1) maker expression (western-blot) was almost completely reversed by pre-treatment with SB203580 (SB) (5μM), a pharmacologic inhibitor of p38α/β. Data is presented as percent of vehicle control. (**D**) G2.2's (100 μM) inhibition of HT-29 CSC self-renewal (3° spheroids) is completely attenuated in the presence of p38α siRNA (KD) compared to scrambled controls. (**E & F**) Similarly, G2.2 caused inhibition of (**E**) HT-29 and (**F**) HCT 116 CSC self-renewal (3° spheroids) is near-completely attenuated in the presence of p38α agf (a p38 dominant negative) compared to scrambled controls. Error bars represent ±1 SEM. ¶p-value < 0.005 compared to vehicle control. §p-value < 0.005 compared to G2.2.

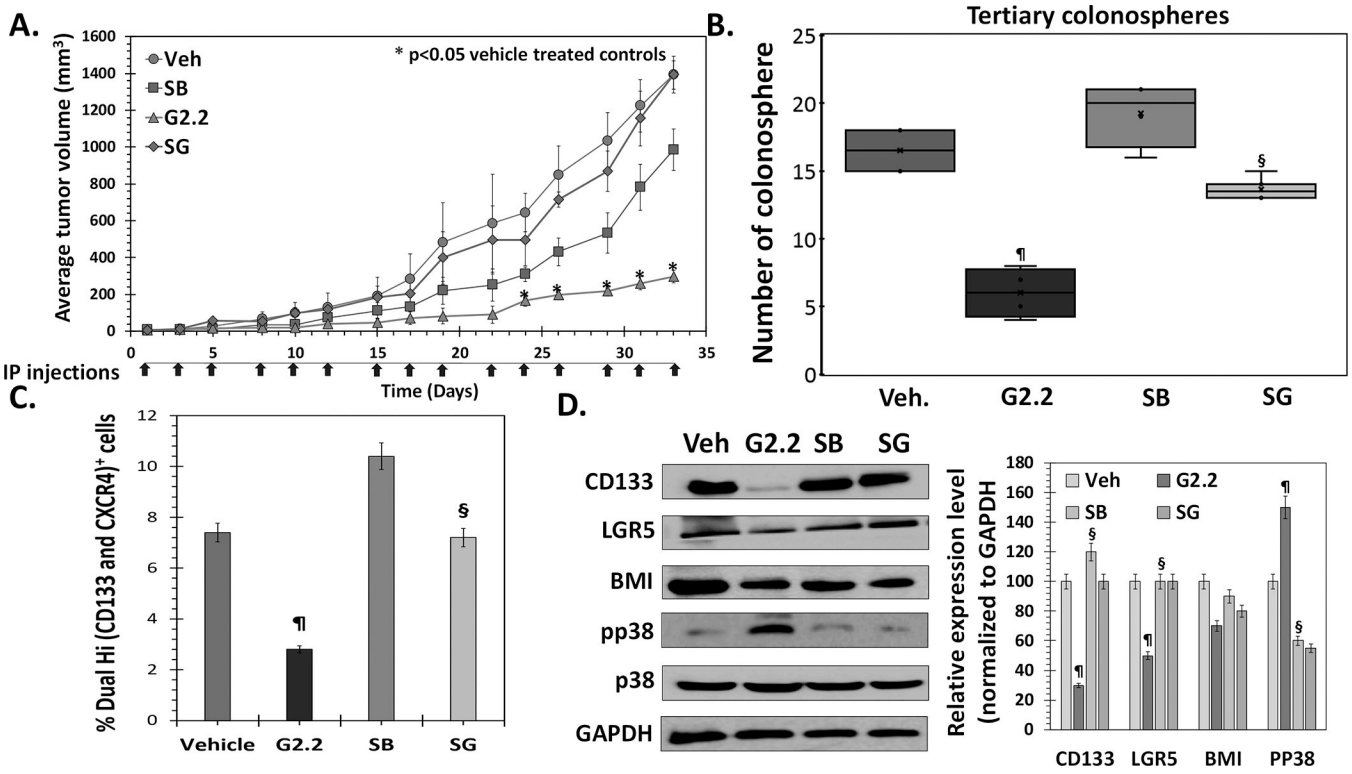

Figure 5: G2.2 inhibits colon CSCs *in vivo* through p38 activation-dependent mechanism.

(**A**) Average tumor volume of Dual hi HT-29 induced s.c. xenografts treated with 1. Veh, 2. G2.2 (schedule), 3. SB (schedule) (p38 α/β inhibitor) 4. SB 3-hours prior to G2.2 (SG) indicates reversal of tumor volume inhibition induced by G2.2 in the presence of pre-treatment with SB. (**B)** G2.2 induced inhibition of CSC self-renewal (3° sphere formation) in xenograft-derived cells was almost completely reversed by pre-treatment with SB. Interestingly, treatment with SB alone resulted in increase in CSC self-renewal despite modest tumor volume reduction suggesting a role of p38 in inversely regulating CSCs. (**C**) Flow cytometry analysis (bar-graph representation) of the proportion of Dual (hi) cells in xenografts demonstres the role of SB in reversing the CSC inhibition by G2.2. **(D)** Western blot analyses and the corresponding bar graph representation of relative densitometry values normalized to GAPDH (housekeeping protein) of CSC (CD133, LGR5)/ self-renewal (BMI1) markers as well as pp38 levels shows complete reversal of G2.2's effects in mice treated with SB>G2.2 treatment. Error bars represent ±1 SEM. *p-value < 0.05 compared to vehicle treated control. ¶p-value <0.005 compared to vehicle. §p-value < 0.005 compared to G2.2.

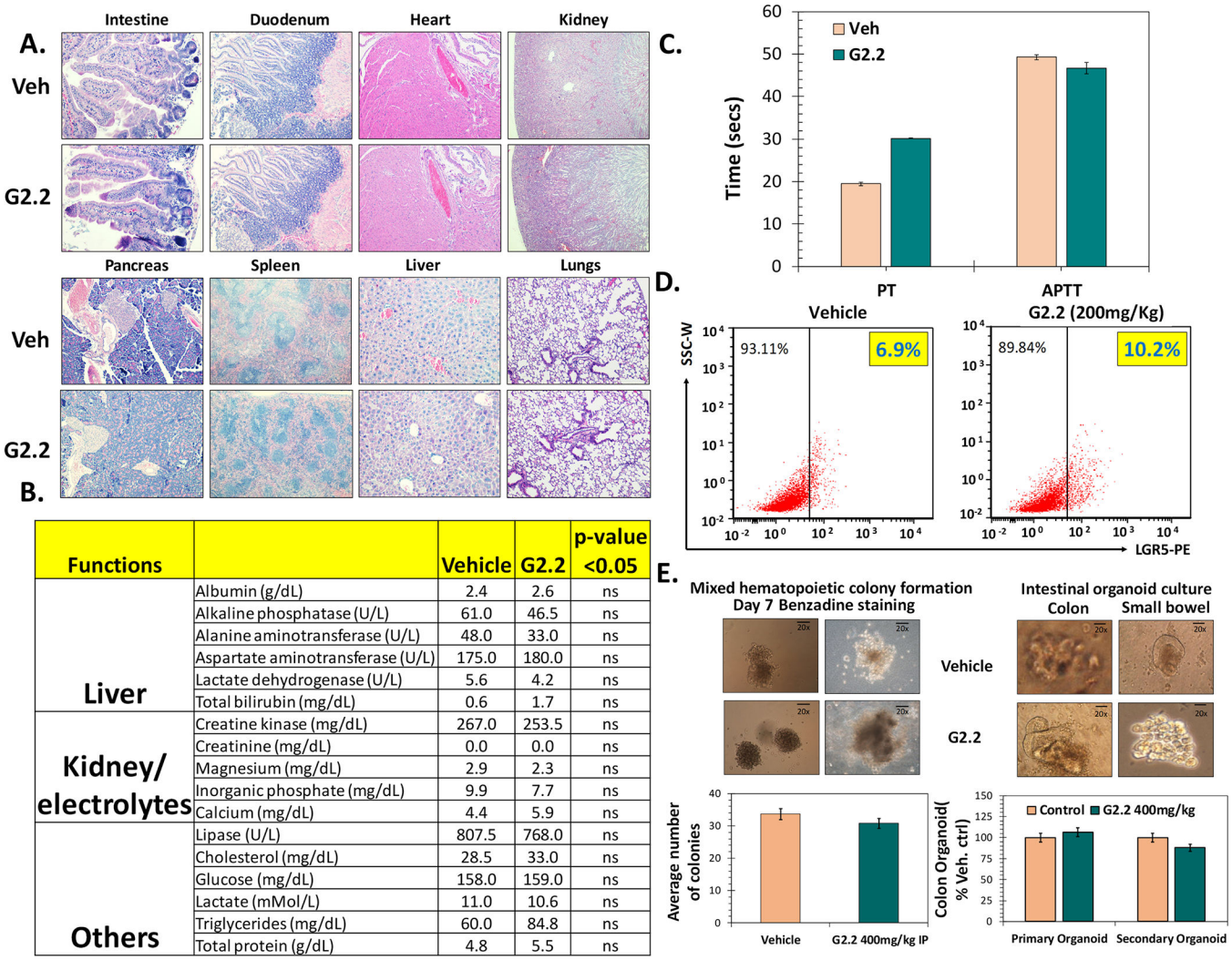

Functions		Vehicle	G2.2	p-value <0.05
Liver	Albumin (g/dL)	2.4	2.6	ns
	Alkaline phosphatase (U/L)	61.0	46.5	ns
	Alanine aminotransferase (U/L)	48.0	33.0	ns
	Aspartate aminotransferase (U/L)	175.0	180.0	ns
	Lactate dehydrogenase (U/L)	5.6	4.2	ns
	Total bilirubin (mg/dL)	0.6	1.7	ns
Kidney/ electrolytes	Creatine kinase (mg/dL)	267.0	253.5	ns
	Creatinine (mg/dL)	0.0	0.0	ns
	Magnesium (mg/dL)	2.9	2.3	ns
	Inorganic phosphate (mg/dL)	9.9	7.7	ns
	Calcium (mg/dL)	4.4	5.9	ns
Others	Lipase (U/L)	807.5	768.0	ns
	Cholesterol (mg/dL)	28.5	33.0	ns
	Glucose (mg/dL)	158.0	159.0	ns
	Lactate (mMol/L)	11.0	10.6	ns
	Triglycerides (mg/dL)	60.0	84.8	ns
	Total protein (g/dL)	4.8	5.5	ns

Figure 6: G2.2 exhibits none to minimal untoward effects on key organs or adult stem/progenitor cell function in nude mice.

(A) Photomicrographs representative of histochemical analyses (H&E stain) of vital organs harvested from vehicle and G2.2 (200 mg/kg dose 3×/wk for 5 weeks) treated animals. (**B**) Bar graph representation of serum biochemical parameters indicating no substantial damage to key organs (e.g. liver, kidney, muscles etc.) and/or their function by G2.2 treatment (200 mg/kg 3×/wk for 5 weeks) compared to vehicle controls. (**C**) Bar graph representation of changes in PT and PTT in serum of vehicle and G2.2 (200 mg/kg 3×/wk for 3 weeks) treated animals show a modest prolongation of PT (< 2-fold) but not PTT by G2.2. (**D**) Flow cytometry analyses of mice intestinal mucosal cells for NSC marker LGR5 demonstrating lack of toxicity of G2.2 (200 mg/kg for 3×/wk 3 weeks). **(E)** Photomicrographs and associated bar graph quantitation representing organoid/colony growth show lack of toxicity of G2.2 (400 mg/kg for 3×/wk for 3 weeks) on proliferation of colonic (organoids), and bone-marrow (mixed colonies) derived stem/progenitor cells compared to vehicle controls. Error bars represent ±1 SEM.